

Inferring Zonal Wind Profiles in the Equatorial Electrojet From Coherent Scatter

D. L. Hysell, J. L. Chau, J. F. Conte, R. Flores, and M. A. Milla

Abstract – Zonal wind estimates in the equatorial electrojet derived from coherent scatter echoes, specular meteor trail echoes, and optical limb scans are compared. While the three techniques exhibit broad overall agreement, significant differences in the results of the three techniques appear. The differences can be attributed in large part to horizontal inhomogeneity in the winds and the dissimilar averaging kernels of the three techniques.

1. Introduction

The thermospheric winds in the equatorial E region shape the electrojet and influence the instabilities and irregularities within [15]. However, measuring altitude-resolved winds in the electrojet (~ 95 km to 110 km altitude) and assessing their role is difficult. Coherent scatter from small-scale irregularities in the electrojet is a source of intense radar clutter, which prevents the use of the incoherent scatter technique in the electrojet region over the Jicamarca Radio Observatory. This is true even when the radar main antenna beam is pointed away from the direction perpendicular to the geomagnetic field because of clutter leaking through the antenna sidelobes [4].

Specular meteor trail echoes offer an incisive method for measuring wind profiles in the equatorial electrojet. However, most specular meteor trails form below the electrojet, and the altitude and time resolution of the specular meteor radar (SMR) techniques are marginal for studying dynamics and stability in the narrow stratum where the electrojet flows [6]. Non-specular meteor trails can be also used for obtaining E region wind profiles with relatively high-altitude resolution. However, wind estimates using these echoes require long-lasting echoes that occur mainly at night [17]. Space-based optical remote sensing of the electrojet is an alternative approach. Here too, however,

altitude resolution is marginal for detailed dynamics and stability studies, and any given region of interest can be observed only once per orbit [14].

[19] introduced a technique for estimating the zonal winds in the equatorial electrojet using coherent scatter from meter-scale plasma density irregularities, which are strong and ubiquitous during the day. The technique was implemented using a low-power radar system at Jicamarca that exploited the strength of the coherent echoes. While the technique appeared to be promising, validation options were limited at the time.

For this study, we reimplemented the technique of [9] at Jicamarca, where zonal wind measurements from the Ionospheric Connection Explorer (ICON) satellite and from the Spread Spectrum Interferometric Multi-static meteor radar Observing Network (SIMONe) system deployed in the vicinity are now available for comparison. Below, we review the method and then compare results from it with wind measurements from ICON and SIMONe acquired in a recent experimental campaign.

2. Electrojet Method

The method involves measuring range-resolved coherent scatter Doppler spectra from small-scale plasma density irregularities in the equatorial electrojet region. The range resolution of the experiment described here is typically about 1 km or less and is obtained with the use of binary phase coding. The measurements are made using an antenna array with a narrow beam (half-power beamwidth $\sim 3^\circ$) directed at an oblique zenith angle, in this case of approximately 55° . In general, the received spectra will be a superposition of so-called type I and type II components, which are associated, respectively, with Farley–Buneman and gradient drift instabilities. The latter component is broader than the former, exhibits a smaller Doppler shift, and is of interest here [10]. These characteristics are used to isolate the type II spectra and estimate their Doppler shifts based on a fitting procedure that models the spectrum as an asymmetric generalized Gaussian function.

For this technique, the Doppler shift of the type II spectral component is assumed to be governed by the real part of the linear dispersion relation for gradient drift instabilities (see, e.g., [11]),

$$\omega = \frac{\mathbf{k} \cdot (\mathbf{v}_e + \psi \mathbf{v}_i)}{1 + \psi} \quad (1)$$

where \mathbf{k} is the scattering wavevector, which is taken to lie in the plane perpendicular to the geomagnetic field,

Manuscript received 16 October 2022.

David Hysell, Department of Earth and Atmospheric Sciences, Cornell University, Ithaca, New York 14853, USA; e-mail: david.hysell@cornell.edu.

Jorge L. Chau, Leibniz Institute of Atmospheric Physics at the University of Rostock, Kühlungsborn, Germany; e-mail: chau@iap-kborn.de.

J. Federico Conte, Leibniz Institute of Atmospheric Physics at the University of Rostock, Kühlungsborn, Germany; e-mail: conte@iap-kborn.de.

R. Flores, Jicamarca Radio Observatory, Instituto Geofísico del Perú, Lima, Peru; e-mail: rflores@igp.gob.pe.

Marco A. Milla, Sección Electricidad y Electrónica, Pontificia Universidad Católica del Perú, Lima, Perú; e-mail: milla.ma@pucp.edu.pe.

and ω/k is the Doppler shift. The \mathbf{v}_e and \mathbf{v}_i are the electron and ion drift velocities, respectively, and ψ is the anisotropy factor defined below. Here, we take the electron velocity to be dominated by the $\mathbf{E} \times \mathbf{B}$ drift and the ion velocity to be dominated by the neutral wind velocity.

The anisotropy factor is

$$\psi = \frac{(v_{en} + v_e^*)/\Omega_e}{\sum_j f_j (\Omega_j / v_{jn})}$$

where the sum is over ion species, f_j is the fraction of species j , and Ω and v refer to the indicated gyrofrequency and collision frequency with neutrals, respectively. The term v_e^* refers to an anomalous electron collision frequency associated with wave-enhanced transport. [20] and [18] derived an expression for the anomalous electron collision frequency parameterized by the local mean-square variations in perturbed electron number density. We utilize their expression and assume that the controlling parameter scales with the background zonal electric field in the electrojet through a scaling constant determined empirically.

The zonal neutral wind affects the Doppler shift of the echoes predicted by (1) locally through the ion velocity term and nonlocally through the electron velocity term, which depends on the dynamo electric field (see, e.g., [15]). We can expand the electric field as ($\mathbf{E} = \mathbf{E}_0 - \nabla\phi$), where \mathbf{E}_0 is the background average zonal electric field and ϕ is the perturbed electrostatic potential that arises to maintain quasi-neutrality. The vertical component of $\nabla\phi$ drives the electrojet.

In order to calculate the electrostatic potential, we solve the quasi-neutrality condition in the plasma: ($\nabla \cdot \mathbf{J} = 0$). We consider Pedersen, Hall, and direct currents together with wind-driven currents, currents due to diffusion, and currents driven by gravity. We neglect diamagnetic currents, which are nearly solenoidal. The transport coefficients controlling the current density involve finite electron-neutral and ion-neutral collision frequencies and were given by [19]. The neutral atmospheric parameters required to populate the coefficients are extracted from the NRLMSIS model [9], and the ion composition is prescribed by IRI-2016 [2]. The plasma number density is taken from the FIRI model, which is part of IRI-2016 [12]. Finally, the geomagnetic field specification is taken from IGRF-13 [11].

The quasi-neutrality condition is a linear elliptic partial differential equation for the electrostatic potential,

$$\begin{aligned} \nabla \cdot (\Sigma \cdot \nabla\phi) \\ = \nabla \cdot [\Sigma \cdot (\mathbf{E}_0 + \mathbf{u} \times \mathbf{B}) - D \cdot \nabla n + \chi \cdot \mathbf{g}] \quad (2) \end{aligned}$$

where Σ is the plasma conductivity tensor, D the diffusivity tensor, and χ a tensor associated with currents due to gravity. We solve that problem fully in three dimensions using a preconditioned conjugate gradient method. The problem is posed in dipole

magnetic coordinates. Neumann boundary conditions are applied on all boundaries except for the upper boundary, where the vertical perturbed electric field is set assuming a perfectly efficient wind-driven dynamo there. See [19] for details.

We neglect both meridional and vertical winds in the modeling. The former do not significantly affect the predicted Doppler shifts and so have no test implications. The latter are presumed to be small, although the presumption merits reexamination. The horizontal winds are furthermore specified in terms of the vertical extensions of the Hough modes derived by [3], which are linearly independent and serve here as an expansion basis. The winds are specified by 10 to 14 expansion coefficients depending on the number of ranges from which radar measurements are available. The coefficients are adjusted to minimize the discrepancy between the measured and predicted Doppler shifts. Wind estimates are reported at altitude intervals consistent with the fine structure available in the Hough functions.

The average background zonal electric field parameter needed to drive this model is derived from coherent backscatter from the so-called 150 km echoes [5]. At Jicamarca, 150 km echoes are observed using a vertically looking beam concurrently with the oblique electrojet observations. Magnetometer data are also acquired concurrently at Jicamarca and at a nearby station in Piura, Peru. The difference in the magnetometer readings from these stations is indicative of the current flowing in the electrojet, which is calculated from the model and compared for consistency.

3. Observations

We present results from June 24 and 25, 2021, when a campaign was under way at Jicamarca. The campaign included the SIMONE system fielded by the Leibniz Institute of Atmospheric Physics and the ICON satellite. ICON cannot normally measure winds directly over Jicamarca because of elevated cosmic radiation near the South Atlantic Anomaly (SAA). During this campaign, ICON was in so-called rLVLH mode and observing the volume over Jicamarca from the north rather than the south, thereby avoiding the SAA. The mode has been used only infrequently.

Zonal wind estimates derived from oblique echoes from the electrojet are shown in Figure 1. The altitude resolution is 700 m, and the time resolution is approximately 5 min. The figures depict winds mainly but not entirely limited to the range ± 100 m/s and with strong vertical shears that evolve gradually over time. The electrojet echoes are not strong enough to support wind estimates outside the universal times shown.

The temporal fluctuations in the wind estimates exceed expectations based on the propagation of statistical errors in the underlying Doppler data. As significant structuring is also present in the 150 km echo and magnetometer measurements on a 5 min timescale, the fluctuations are deemed to be physically significant.

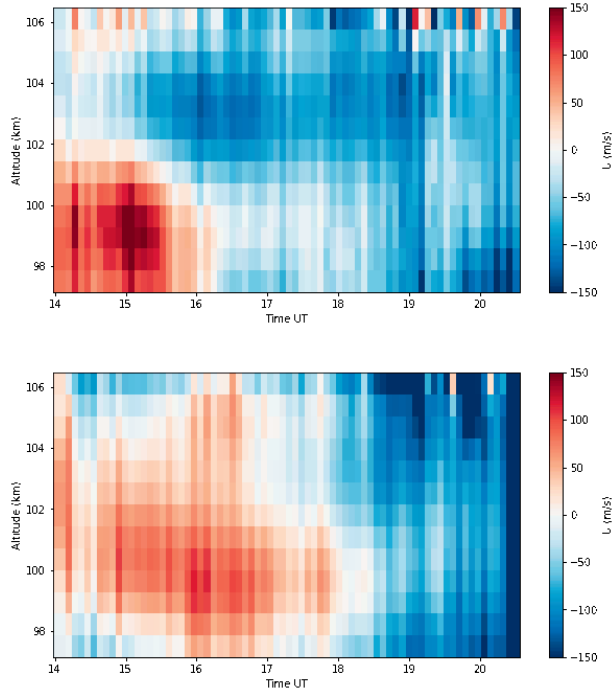


Figure 1. Zonal winds inferred from electrojet observations versus altitude and universal time. Positive values denote eastward winds. Above: June 24, 2021. Below: June 25, 2021.

The principles of operation behind the SIMONE system and the data processing methods were described by [6, 7]. Zonal wind estimates derived from the network from the region surrounding Jicamarca and acquired during the campaign are shown in Figure 2. The altitude and time resolution of the winds estimates are 4 km and 4 h, respectively, oversampled at every 1 km and 1 h. The rectangles in the figures denote the altitude and time coverage of the electrojet wind estimates, which lie at the edge of the zone, where meteor echoes occur frequently enough for reliable wind estimation.

Overall, the SIMONE wind estimates are somewhat smaller than the electrojet-derived estimates, falling entirely within the range ± 100 m/s. The trends in the two data sets are otherwise similar, with winds becoming increasingly westward with increasing altitude and time. The main discrepancy is in the June 24 data set, where the electrojet-derived wind estimates are large and eastward below 102 km altitude before 16 UT, whereas the meteor wind estimates are small and slightly westward.

Finally, Figure 3 compares zonal wind estimates from the Michelson Interferometer for Global High-Resolution Thermospheric Imaging (MIGHTI) green-line instrument on ICON with the electrojet-derived wind estimates [13]. The comparisons are made during conjunctions when the volume probed by MIGHTI shared Jicamarca's longitude. Four conjunctions occurred on each day of the campaign, although MIGHTI data are not available for the first conjunction on June

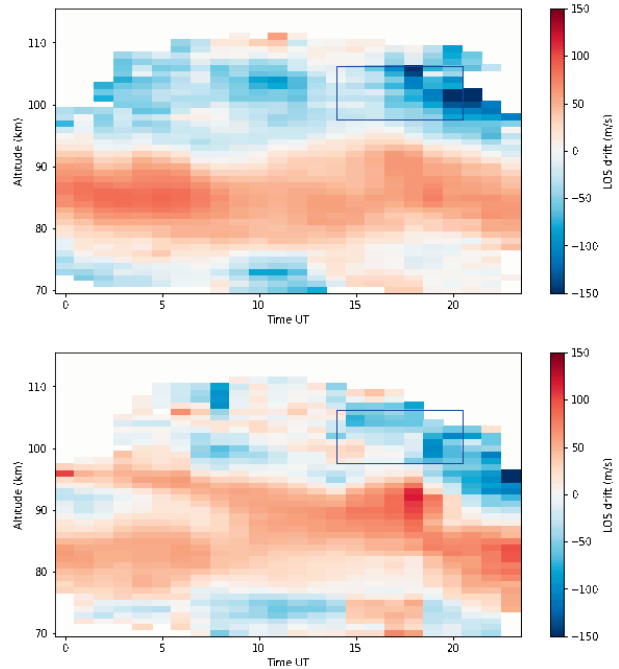


Figure 2. Zonal winds inferred from SIMONE observations versus altitude and universal time. The rectangle indicates the altitude/local time coverage of the electrojet wind estimates. Above: June 24, 2021. Below: June 25, 2021.

24 due to the SAA. The MIGHTI green-line level 2.2 data report values at 30 (60) s time intervals during the daytime (at night) and at ~ 3 km altitude intervals near the electrojet.

Overall, the magnitudes of the zonal winds reported by the MIGHTI green-line instrument are

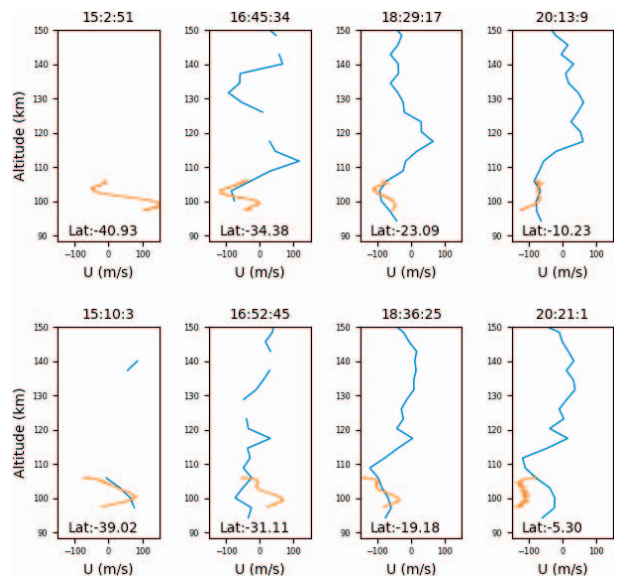


Figure 3. Comparison between ICON (blue) and Jicamarca zonal winds (red). Above: June 24, 2021. Below: June 25, 2021. Annotations give the latitudes of the volumes probed. Data in the first column are contaminated by the SAA.

comparable to electrojet wind estimates. The agreement between them during the June 24 conjunctions is reasonable, although there are discrepancies, comparable in size with those reported in earlier comparisons between MIGHTI and specular meteor radars [14]. The discrepancies are most significant at the lowest altitudes in the electrojet. Only the last of the four conjunctions was a true conjunction in the sense that the volume probed by the MIGHTI instrument had a latitude close to Jicamarca (-11.95°). That the congruity between the measurements was reasonable even when the disparity in latitude was substantial implies latitudinal homogeneity in the wind field on this day.

The agreement between the electrojet-derived and the MIGHTI zonal wind estimates on June 25 was relatively poor by comparison except possibly at the highest altitudes in the electrojet. None of the four conjunctions were close in latitude, however. The 1836 UT conjunction was the closest, and the agreement between the electrojet-derived and MIGHTI measurements during this conjunction was the best. That the electrojet and the SIMONE wind measurements were broadly similar throughout June 25, 2021, suggests that the wind field could have varied significantly in latitude on this day.

4. Analysis and Interpretation

Three means of estimating the zonal winds in the equatorial electrojet have been compared with data from a joint campaign in June 2021. All three are alike in that they are indirect and necessitate the use of inverse methods that involve some degree of regularization. They differ in their observing modality, their spatiotemporal resolution, and underlying assumptions about the stationarity and homogeneity of the wind field.

The temporal resolution of the SIMONE wind estimates is very coarse compared to the MIGHTI and electrojet wind estimates, and this contributes to the relatively small range of absolute wind speeds reported by SIMONE. As MIGHTI vector wind estimates are derived from two line-of-sight measurements made 5 min to 8 min apart, temporal fine structure at intervals comparable to this figure is also lost or misconstrued. The altitude resolutions of the three data sets are comparable, although the MIGHTI wind profiles cannot reproduce the kilometer-scale fine structure evident in the radar-based estimates [9].

A more subtle issue is the size of the volume being probed by the three instruments. The coherent scatter radar probes very small ionospheric volumes with dimensions of the order of a cubic kilometer. However, the zonal winds affect the Doppler shift measurements both locally and nonlocally through the ion and electron contributions to (2). The boundary-value problem represented by (2) predicts the dynamo electric field that drives the electrons as a function of the zonal wind profile, but the inverse methodology assumes that the winds are horizontally uniform across

the electrojet between approximately $\pm 5^\circ$ in magnetic latitude or about 1,100 km in the equatorial E region.

Similar issues apply to the SIMONE and MIGHTI green-line wind estimates. [14] compared the effective horizontal resolution of the MIGHTI green-line measurements and wind measurements from SMRs in China and India. They estimated a 2σ effective horizontal kernel resolution of 200 km to 300 km for the SMRs and 760 km to 1,200 km for MIGHTI green-line measurements.

[16] measured E region wind profiles at two locations near the magnetic equator separated meridionally by 450 km directly with chemical releases. Pairs of releases were performed on two consecutive days. The results were consistent, showing substantial turning in the wind directions between the two locations. The persistent, steep latitudinal gradient in the horizontal wind led the authors to argue that the winds could not be attributed mainly to low-order tidal modes. The horizontal winds in the lower thermosphere are inhomogeneous as a rule, and methods with different horizontal averaging kernels can be expected to yield different results. The differences are aggravated by the fact that the geometries of the averaging kernels in Abel inversion (MIGHTI), radar interferometry (SIMONE), and dynamo electric field forward modeling (electrojet backscatter) are inherently different.

With the electrojet technique, the dipole magnetic field line geometry is such that the higher the apex altitude, the larger the averaging kernel in latitudinal extent. Furthermore, the contribution of the local winds to the Doppler shift predicted by (1) increases with decreasing altitude. Consequently, the electrojet wind estimates represent local estimates at low altitudes and increasingly nonlocal estimates at higher altitudes in the electrojet. To the extent that horizontal gradients are significant, we should expect the electrojet-derived wind estimates to depart from the other estimates. This suggests a method for assessing inhomogeneity in the winds and possibly for making more localized wind estimates on the basis of the discrepancies.

5. Acknowledgments

This project is supported by NASA award 80NSSC22K0015 to Cornell University. The Jicamarca Radio Observatory is a facility of the Instituto Geofísico del Perú operated with support from NSF award AGS-1732209 through Cornell. The help of the staff is much appreciated. SIMONE at Jicamarca is operated in cooperation with the Instituto Geofísico del Perú and Ciencia Internacional. The work of J. F. Conte is supported by the Bundesministerium für Bildung und Forschung via project WASCLIM-IAP, part of the ROMIC-II program. Data used for this publication are available through the Madrigal and ICON databases (see <http://www.openmadrigal.org> and <https://icon.ssl.berkeley.edu/Data>). The authors appreciate the assistance of the ICON team in preparing this manuscript.

6. References

1. P. Alken, E. Thébault, and C. D. Beggan, "International Geomagnetic Reference Field: The Thirteenth Generation," *Earth, Planets, and Space*, **73**, 2021, doi: 10.1186/s40623-020-01288-x.
2. D. Bilitza, D. Altadill, B. Reinisch, I. Galkin, V. Shubin, et al., "The International Reference Ionosphere: Model Update 2016," in *EGU General Assembly Conference Abstracts*, **18**, 2016, p. 9671.
3. S. Chapman and R. S. Lindzen, *Atmospheric Tides Thermal and Gravitational*, Dordrecht, D. Reidel, 1970.
4. J. L. Chau and E. Kudeki, "First E- and D-Region Incoherent Scatter Spectra Observed Over Jicamarca," *Annales Geophysicae*, **24**, 5, 2006, pp. 1295-1303, doi: 10.5194/angeo-24-1295-2006.
5. J. L. Chau and R. F. Woodman, "Daytime Vertical and Zonal Velocities From 150-km Echoes: Their Relevance to F-Region Dynamics," *Geophysical Research Letters*, **31**, 2004, p. L17801, doi: 10.1029/2004GL020800.
6. J. L. Chau, J. M. Urco, J. Vierinen, B. J. Harding, M. Clahsen, et al., "Multistatic Specular Meteor Radar Network in Peru: System Description and Initial Results," *Earth and Space Science*, **1**, 2021, p. e01293, doi: 10.1029/2020EA001293.
7. J. F. Conte, J. L. Chau, J. M. Urco, R. Latteck, J. Vierinen, et al., "First Studies of Mesosphere and Lower Thermosphere Dynamics Using a Multistatic Specular Meteor Radar Network Over Southern Patagonia," *Earth and Space Science*, **8**, 2021, doi: 10.1029/2020EA001356.
8. J. T. Emmert, D. P. Drob, M. Picone, D. E. Siskind, M. Jones Jr., et al., "NRLMSIS 2.0: A Whole-Atmosphere Empirical Model of Temperature and Neutral Species Densities," *Earth and Space Science*, **8**, 2021, doi: 10.1029/2020EA001321.
9. S. L. England, C. R. Englert, B. J. Harding, C. C. Triplett, K. Marr, et al., "Vertical Shears of Horizontal Winds in the Lower Thermosphere Observed by ICON," *Geophysical Research Letters*, **49**, 2022, doi: 10.1029/2022GL098337.
10. D. T. Farley, "The Equatorial E-Region and Its Plasma Instabilities: A Tutorial," *Annales Geophysicae*, **4**, 2009, pp. 1509-1520, doi: 10.5194/angeo-27-1509-2009.
11. B. G. Fejer and M. C. Kelley, "Ionospheric Irregularities," *Reviews of Geophysics*, **18**, 1980, pp. 401-454.
12. M. Friedrich and K. Tokar, "FIRI: A Semiempirical Model of the Lower Ionosphere," *Journal of Geophysical Research*, **106**, A10, 2001, pp. 21409-21418.
13. B. J. Harding, J. J. Makela, C. R. Englert, K. D. Marr, J. M. Harlander, et al., "The MIGHTI Wind Retrieval Algorithm: Description and Verification," *Space Science Reviews*, **212**, 2017, pp. 585-600, doi: 10.1007/s11214-017-0359-3.
14. B. J. Harding, J. L. Chau, M. He, C. R. Englert, J. M. Harlander, et al., "Validation of ICON-MIGHTI Thermospheric Wind Observations: 2. Green-Line Comparisons to Specular Meteor Radars," *Journal of Geophysical Research*, **126**, 2021, doi: 10.1029/2020JA028947.15. D. L. Hysell, J. L. Chau, and C. G. Fesen, "Effects of Large Horizontal Winds on the Equatorial Electrojet," *Journal of Geophysical Research*, **107**, 2002, doi: 10.1029/2001JA000217.
15. M. F. Larsen and C. D. Odom, "Observations of Altitudinal and Latitudinal E-Region Neutral Wind Gradients Near Sunset at the Magnetic Equator," *Geophysical Research Letters*, **24**, 1997, pp. 1711-1714.
16. M. M. Oppenheim, G. Sugar, N. Slowey, O. Nicholas, E. Bass, et al., "Remote Sensing Lower Thermosphere Wind Profiles Using Non-Specular Meteor Echoes," *Geophysical Research Letters*, **9**, 2009, pp. 1-5, doi: 10.1029/2009GL037353.
17. C. Ronchi, R. N. Sudan, and P. L. Similon, "Effect of Short-Scale Turbulence on Kilometer Wavelength Irregularities in the Equatorial Electrojet," *Journal of Geophysical Research*, **95**, 1990, pp. 189-200.
18. E. B. Shume, D. L. Hysell, and J. L. Chau, "Zonal Wind Velocity Profiles in the Equatorial Electrojet Derived From Phase Velocities of Type II Radar Echoes," *Journal of Geophysical Research*, **110**, 2005, doi: 10.1029/2005JA011210.
19. J. P. St-Maurice, "A Unified Theory of Anomalous Resistivity and Joule Heating Effects in the Presence of Ionospheric E Region Irregularities," *Journal of Geophysical Research*, **92**, 1987, pp. 4533-4542.